molecular pharmaceutics

pubs.acs.org/molecularpharmaceutics Article

Reduction of Punch-Sticking Propensity of Celecoxib by Spherical Crystallization via Polymer Assisted Quasi-Emulsion Solvent Diffusion

Hongbo Chen, Shubhajit Paul, Hongyun Xu, Kunlin Wang, Mahesh K. Mahanthappa, and Changquan Calvin Sun*

Cite This: *Mol. Pharmaceutics* 2020, 17, 1387−1396 Read Online

ACCESS | Metrics & More | Article Recommendations | Supporting Information

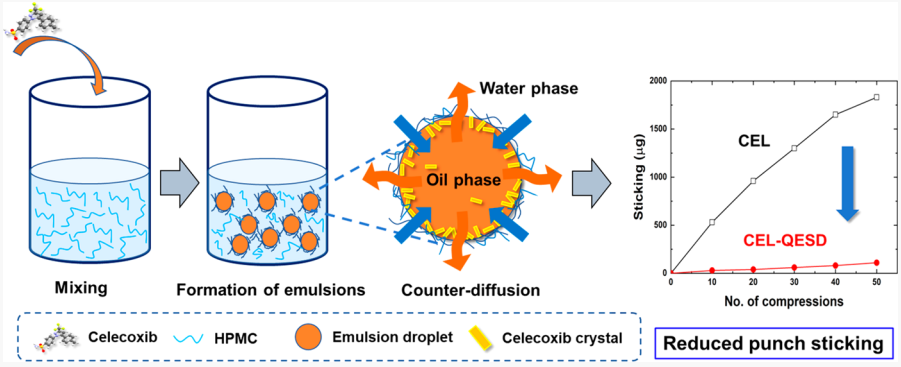

ABSTRACT: Punch-sticking during tablet compression is a common problem for many active pharmaceutical ingredients (APIs), which renders tablet formulation development challenging. Herein, we demonstrate that the punch-sticking propensity of a highly sticky API, celecoxib (CEL), can be effectively reduced by spherical crystallization enabled by a polymer assisted quasi-emulsion solvent diffusion (QESD) process. Among three commonly used pharmaceutical polymers, poly(vinylpyrrolidone) (PVP), hydroxypropyl cellulose (HPC), and hydroxypropyl methylcellulose (HPMC), HPMC was the most effective in stabilizing the transient emulsion during QESD and retarding the coalescence of emulsion droplets and the initiation of CEL crystallization. These observations may arise from stronger intermolecular interactions between HPMC and CEL, consistent with solution ^{1}H NMR analyses. SEM and X-ray photoelectron spectroscopy confirmed the presence of a thin layer of HPMC on the surfaces of spherical particles. Thus, the sticking propensity was significantly reduced because the HPMC coating prevents direct contact between CEL and the punch tip during tablet compression.

KEYWORDS: *punch sticking, spherical crystallization, surface coating, Celecoxib, HPMC*

INTRODUCTION

Several powder properties of active pharmaceutical ingredients (APIs), such as tabletability, flowability, bulk density, and punch-sticking propensity are critical for efficient and successful tablet formulation design, especially at high drug loadings (>30% w/w).[1−3] The punch-sticking propensity refers to the tendency of the API powder to adhere to the punch tip during tablet compression. Relative to other powder properties, the punch-sticking propensity of an API is rarely evaluated during early stage therapeutic development, even though it is a well-recognized and common problem in tablet manufacturing that adversely affects the aesthetic qualities of a finished tablet product.[4−6] Punch sticking is influenced by process variables such as tableting speed, compaction pressure,[7] tooling material,[8] and tooling design,[9] as well as API material properties, including mechanical properties,[10] surface chemistry,[10] particle sizes,[7] and choice of excipients.[11] As compared to modifying tablet compaction tooling, the elimination of punch sticking through formulation approaches is more desirable to ensure tablet quality because of its economy, effectiveness, and broad applicability.

Among the formulation techniques that have been pursued to reduce the punch-sticking propensity, crystal engineering presents an attractive approach as it addresses the root cause, instead of the symptoms, of API deficiency by altering the API crystal structure and its consequent material properties. For

Received: January 27, 2020
Revised: March 4, 2020
Accepted: March 5, 2020
Published: March 5, 2020

https://dx.doi.org/10.1021/acs.molpharmaceut.0c00086
Mol. Pharmaceutics 2020, 17, 1387−1396

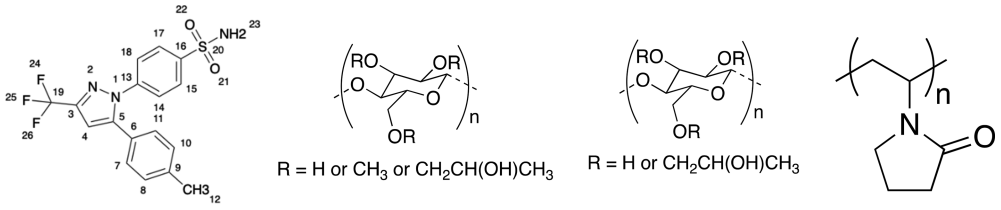

Figure 1. Chemical structures of (a) the model API CEL and commonly used polymeric stabilizers (b) HPMC, (c) HPC, and (d) PVP.

example, salt formation can reduce the punch-sticking propensity by altering the mechanical properties and surface chemistries of crystalline APIs.[10,12] When crystal engineering through structure modifications is not possible, another effective approach to address API punch sticking is particle engineering through processes, such as mixing with suitable excipients[11] and dry granulation.[13] Quasi-emulsion solvent diffusion (QESD) is a particle engineering process for preparing spherical agglomerates (SA) consisting of fine API crystals.[14] QESD has been employed to improve flowability, bulk density, tabletability, and dissolution characteristics of APIs.[15−19] However, it remains unclear whether API engineering by QESD can be used to overcome the punch-sticking problem.

Celecoxib (CEL) is a COX-2 selective, nonsteroidal anti-inflammatory drug for treating chronic pain and inflammation associated with osteoarthritis, rheumatoid arthritis, and other acute pain symptoms in adults.[20] The commercial CEL crystal (Form III), which exhibits high one-dimensional elasticity,[21] is a challenging API for tablet formulation development because of its significant punch-sticking propensity.[4] In this work, we explore the specific use of QESD as a means to reduce the punch-sticking propensity of CEL. Our studies reveal that QESD processing with (hydroxypropyl)methyl cellulose (HPMC) can reduce CEL punch-sticking propensity, while simultaneously improving its tabletability and flowability, by forming spherical HPMC-coated CEL crystals.

MATERIALS AND METHODS

Materials. Celecoxib (CEL, Form III, Aarti Pvt Ltd., Mumbai, India), microcrystalline cellulose (Avicel PH102, FMC, Philadelphia, PA), HPMC (K15M, MW 575 000 g/mol, Ashland Specialty Ingredients, Wilmington, DE), HPC (EF Pharm, MW 80 000 g/mol, Ashland Specialty Ingredients, Wilmington, DE), PVP (90F, MW 1 000 000−1 500 000 g/mol, BASF, Ludwigshafen, Germany), magnesium stearate (MgSt, Mallinckrodt Inc., St. Louis, MO), ethyl acetate (EA, Sigma-Aldrich, St. Louis, MO), ultrapure deionized water (0.066 μS/cm, Thermo Scientific, Waltham, MA) were used as received. The chemical structures of CEL, HPMC, HPC, and PVP are given in Figure 1. All crystallization experiments were performed in glass beakers at the specified temperatures.

Methods. *Polymer Screening for Quasi-Emulsion Solvent Diffusion (QESD).* Ethyl acetate (EA) and water were selected as good and poor solvents for the QESD process because the two solvents are somewhat miscible and the solubility of CEL is high in EA and low in water. A solution containing 3 g of CEL in 9 mL of EA at 70 °C was added dropwise to 70 mL of an aqueous solution of 0.5% (w/w) polymer (HPMC, HPC, or PVP) at 22 °C to form spherical agglomerates over 3 min. The mixture was agitated at 600 rpm using an overhead mixer. Spherical agglomerates were captured on filter paper (Fisher Scientific, Pittsburgh, PA) supported with a Brinell funnel after 15 min when the suspension no longer appeared to change, and they were dried at 60 °C overnight in an oven. The morphology of produced agglomerates was assessed to guide the selection of more appropriate polymer additives.

QESD Spherical Agglomerate Growth Kinetics. An 0.9 mL aliquot of a 0.33 mg/mL CEL solution in EA at 70 °C was added at once to a 7 mL of a 0.5% (w/w) polymer (HPMC, HPC, or PVP) aqueous solution under 600 rpm agitation using a magnetic stir bar at room temperature. The time-dependence of the QESD process was monitored in increments appropriate to the rates of drop solidification associated with the different polymer additives. At each time point, a small volume of suspension (less than 1 mL) was withdrawn using a disposable plastic pipet and immediately transferred onto a glass slide for imaging under a polarized light microscope (Eclipse E200; Nikon, Tokyo, Japan).

Particle Size Distribution. Particle size distribution measurement of CEL and CEL-QESD was carried out using a particle size analyzer (Microtrac SIA, Montgomeryville, PA). Each powder (∼50 mg) was suspended in Isopar G Fluid (∼10 mL), in which the solubilities of CEL and polymers are negligible. The suspension was added dropwise into a sample delivery controller (SDC, Montgomeryville, PA) until the particle density reached the acceptable range for each measurement. A high-speed camera captured image of particles in focus, from which the area equivalent diameter of each particle was determined using image analysis software (Microtrac Flex) provided with the instrument. All experiments were performed in triplicate.

Powder X-ray Diffractometry (PXRD). Crystallographic properties of samples were characterized using a X'Pert PRO powder X-ray diffractometer (PANalytical Inc., West Borough, MA) equipped with a copper X-ray source (45 kV and 40 mA) to provide K_α radiation (1.5406 Å) over the angular range $5° \leq 2\theta \leq 35°$ using a 0.017° step size and a dwell time of 1.15 s. The divergence and anti-scattering slits on the incident beam path were 1/16 and 1/8 degree, respectively, and the anti-scattering slit on the diffracted beam path was 5.5 mm (X'Celerator). The expected PXRD pattern of CEL Form III was calculated from its crystal structure.[21]

Thermal Analyses. Powder samples (3−5 mg) were loaded into hermetically sealed, aluminum pans and heated from 20 to 180 °C at a rate of 10 °C/min on a Q1000 differential scanning calorimeter (DSC, TA Instruments, New Castle, DE) under a continuous nitrogen purge at a flow rate of 50 mL/min. The DSC cell temperature was calibrated with both indium and cyclohexane, and the heat flow cell parameter was calibrated using the indium standard. To measure the residual volatile content in the solids obtained by QESD, thermogravi-

https://dx.doi.org/10.1021/acs.molpharmaceut.0c00086
Mol. Pharmaceutics 2020, 17, 1387−1396

metric analyses were performed using a Q500 Thermogravimetric Analyzer (TA Instruments, New Castle, DE). Solid samples (~3−10 mg) were placed in an open aluminum pan and heated from 22 to 300 °C at a rate of 10 °C/min under 25 mL/min nitrogen gas purge.

True Density Measurement. The true density of CEL was measured using a helium pycnometer (Quantachrome Instruments, Ultrapycnometer 1000e, Byonton Beach, FL). Accurately weighed powders (1−2 g) were filled into the sample cell. The sample volume was measured repeatedly until the coefficient of variation of the last five consecutive measurements was below 0.005%. The mean and standard deviation of the last five measurements were calculated and reported. The true density of CEL-QESD was assumed to be the same as CEL since the amount of HPMC in CEL-QESD was small and the density difference between HPMC and CEL is also small.

Powder Flowability, Tabletability, and Punch-Sticking Assessment. A ring shear cell tester (RST-XS; Dietmar Schulze, Wolfenbüttel, Germany) with a 10 mL cell was used to assess powder flowability at a 1 kPa preshear normal stress. A yield locus was obtained by conducting shear test under different normal stresses (0.25, 0.40, 0.55, 0.70, and 0.85 kPa), from which the unconfined yield strength (f_c) and major principal stress (σ_n) were obtained by drawing Mohr's circles. The flowability index (ff_c) was calculated using eq 1.

$$ff_c = \frac{\sigma_n}{f_c} \tag{1}$$

Tabletability was analyzed for both pure components and formulations. Tablets were prepared by single-sided compression at compaction pressures ranging 50−300 MPa using a Universal Material Testing Machine (Model 1485, Zwick/Roell, Germany) at a speed of 4 mm/min. A 5% (w/v) suspension of MgSt in ethanol was used to coat the punch tip and die wall, which was air-dried with a fan for ~1 min to complete dryness. Tablets were allowed to relax under ambient conditions for at least 24 h prior to being broken diametrically using a Texture Analyzer (TA-XT2i, Texture Technologies Corporation, Scarsdale, NY). Tablet flashing was carefully removed to improve the accuracy of measured tablet thickness.[22] Tablet tensile strength was calculated from the breaking force (F), tablet thickness (h), and tablet diameter (d) according to eq 2.[23]

$$\sigma = \frac{2F}{\pi dh} \tag{2}$$

Punch-sticking propensity was assessed using formulations consisting of 79.5% (w/w) of Avicel PH102, 20% (w/w) of CEL, and 0.5% (w/w) of MgSt on a Presster Compaction Simulator (Measurement Control Corp., East Hanover, NJ) with a 12.7 mm diameter flat-faced upper punch with a removable tip (tare weight 3 g). A total of 50 tablets were compressed at 250 MPa with a dwell time of 25 ms, simulating a Korsch XL100 press (10 stations) operating at a production rate of 49 300 tablets/h. The punch tip was removed and weighed with precision of 0.01 mg after making every 10 tablets to determine the punch-sticking kinetics, and the mean weight gain over three independent weight measurements was plotted against the number of compressions.

Compressibility and Compactibility Analyses. Compressibility, which is derived from a plot of tablet porosity as a function of compaction pressure, indicates the extent of powder volume reduction under a given compaction pressure. Porosity of the compacts (ε) was calculated from tablet density (ρ_c) and true density (ρ_t = 1.4833 ± 0.0004 g/cm^3 for CEL) of the material using eq 3.

$$\varepsilon = 1 - \rho_c/\rho_t \tag{3}$$

Compactibility, which is derived from a plot of σ as a function of ε, was analyzed by nonlinear regression according to eq 4.[24]

$$\sigma = \sigma_0 e^{-b\cdot\varepsilon} \tag{4}$$

where σ_0 is the tablet tensile strength at zero porosity and b is a constant, which represents the sensitivity of σ to a change in ε.

Scanning Electron Microscopy (SEM). Samples were mounted onto carbon tapes and sputter-coated with a thin layer of platinum (thickness ~75 Å) using an ion-beam sputter (IBS TM200S, VCR Group Inc., San Clemente, CA). Particle morphology and surface features were evaluated using a JEOL 6500F scanning electron microscope (JEOL Ltd., Tokyo, Japan), operated at SEI mode with an acceleration voltage of 5 kV under a high vacuum (10^{-4}−10^{-5} Pa) during imaging.

X-ray Photoelectron Spectroscopy (XPS). The XPS measurements were performed using a PHI Versa Probe III XPS system (ULVAC-PHI; Physical Electronics, Inc., Chanhassen, MN, USA) with monochromated Al Kα X-ray source (1486.6 eV, power of 50 W under 15 kV) with a base pressure of 5.0 × 10^{-8} Pa and a 0.2 mm diameter X-ray spot size. During data collection, the pressure in the sample chamber was maintained near 1.0 × 10^{-6} Pa. Samples were mounted on a stainless steel holder using carbon tape. Tablet samples were mounted in such a way that the surface of interest faced upward for elemental analysis. Charge neutralization was used since the materials are electrically nonconductive. The incidence angle of X-ray was 90°, and takeoff angle of electrons was 45°. The pass energy used was 280 eV with a 1.0 eV/step. Atomic percentages were calculated from the average survey spectrum (n = 3) using the Multipak software provided with the XPS system.

HPMC Content Determination. The HPMC content in CEL samples prepared by QESD was determined by size-exclusion chromatography (SEC) using an Agilent 1260 liquid chromatograph (LC) operating with an aqueous mobile phase containing 0.1 M Na_2SO_4 and 1 wt % acetic acid at a flow rate of 0.4 mL/min. The SEC was equipped with one guard column and three CATSEC separation columns with pore sizes of 1000, 300, and 100 Å, respectively. Analyte detection by an inline Wyatt Optilab T-rEX refractive-index detector (Wyatt Technologies, Santa Barbara, CA) enabled HPMC concentration determination from the peak area corresponding to polymer fraction in the ASTRA software.[25,26] The refractive index increment was dn/dc = 0.1165 mL/g for HPMC under the analysis conditions, which was determined by SEC analyses of HPMC (K15M) solutions of known concentrations assuming 100% mass recovery. For each measurement, CEL-QESD powder (0.65 g) was dissolved in 5 mL of HPLC grade tetrahydrofuran (THF), in which the HPMC precipitated out. The precipitate was then isolated by centrifugation force at 11 644g for 10 min, and the CEL solution in THF was carefully decanted. In order to remove any residual CEL, the HPMC polymer was redispersed in 5 mL of THF by sonication for 10 min and isolated again by centrifugation. Upon removal of residual THF under a vacuum, the isolated HPMC was dissolved in 5 mL of the aqueous SEC mobile phase and the

https://dx.doi.org/10.1021/acs.molpharmaceut.0c00086
Mol. Pharmaceutics 2020, 17, 1387−1396

concentration was determined by SEC. The reported HPMC content in each CEL-QESD sample represents an average of three independent measurements.

^{1}H NMR Spectroscopy. 1D solution ^{1}H NMR spectra in DMSO-d_6 were acquired at 298 K on a Bruker AV-400 NMR spectrometer (Bruker BioSpin GmbH, Rheinstetten, Germany) operating at a proton resonance frequency of 400 MHz. Chemical shifts were referenced with respect to the residual proton resonance of DMSO-d_6 (2.50 ppm).

RESULTS AND DISCUSSION

Polymer Screening and Granule Growth Process. During the QESD process, the polymer used in aqueous solution significantly influenced the morphology of the resulting agglomerates. The sphericity of the CEL agglomerates qualitatively decreased in the order of HPMC ≫ HPC > PVP ≈ no polymer (Figure 2). The addition of HPMC notably

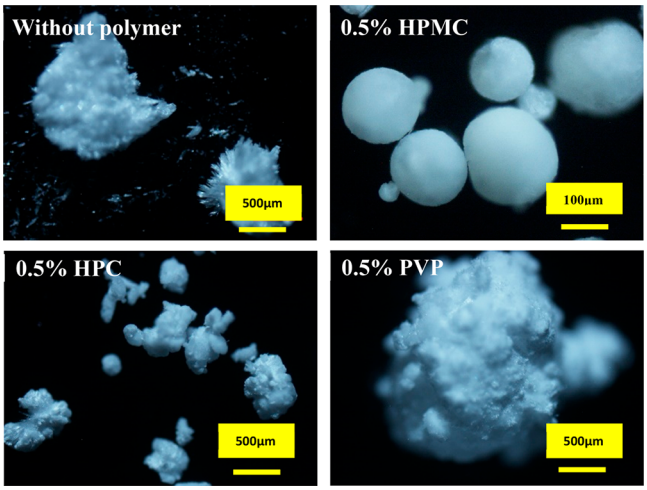

Figure 2. Optical micrographs of agglomerates prepared by QESD method in the absence and presence of various polymers.

led to spherical agglomerates with smooth surfaces, while only irregular agglomerates with rough surfaces were produced in the presence of HPC. The agglomerates produced from PVP solutions were large and even more irregular than those from the HPC solution, in a manner similar to those obtained from QESD without any polymer (Figure 2).

To better understand the origin of the distinct granule morphologies, the time-dependent process of granule growth was monitored for each polymer additive (Figure 3). In all aqueous polymer solutions examined here, emulsions were formed upon addition of CEL solution. The emulsion formed by the HPMC solution was stable for 6 min, after which the phase separated CEL droplets gradually solidified to form spherical agglomerates (Figure 3a). In contrast, emulsions formed in the HPC and PVP solutions were less stable, since crystallization of CEL droplets began after about 1 min and 30 s, respectively (Figure 3b,c). In the PVP solution, coalescence of emulsion droplets also rapidly took place, which led to the formation of large granules (Figure 3c).

Thus, sufficient emulsion stability against coalescence is required for crystallization of the droplets to occur at the surfaces and propagate into the droplet core. This confined crystallization mode results in a spherical particle morphology that mimics that of the parent emulsion droplets. Unstable emulsions, wherein coalescence of small droplets of CEL takes place more quickly than crystallization, leads to the formation of large and irregular agglomerates. Therefore, the crystallization onset time represents a good criterion for selecting appropriate polymers to enable the successful development of a QESD process. Accordingly, the 0.5% (w/w) HPMC, was used in subsequent studies as the crystallization medium to produce high-quality, spherical agglomerates of CEL, designated as CEL-QESD.

Sticking Propensity Reduction by CEL-QESD. During tablet compression, a significant amount of the as-received CEL powder visibly adhered to the punch surface after a single compression (Figure 4a), consistent with the known severe punch-sticking propensity of CEL.[11] In contrast, the CEL-QESD powders exhibited significantly less punch-sticking propensity than as-received CEL. Moreover, the degree of reduction was visually evident as the HPMC concentration in the QESD process increased from 0.1 to 0.5 wt % (Figure 4b–d). The CEL powder prepared from the 0.5% HPMC aqueous

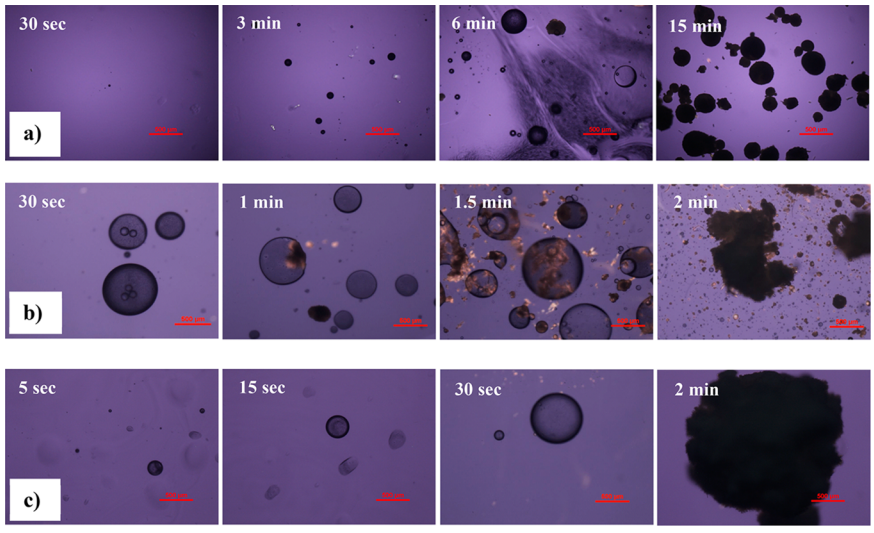

Figure 3. Time-dependent growth of CEL spherical agglomerates in various aqueous polymer solutions assessed by a polarized light microscopy: (a) HPMC, (b) HPC, and (c) PVP. All scale bars are 500 μm.

https://dx.doi.org/10.1021/acs.molpharmaceut.0c00086
Mol. Pharmaceutics 2020, 17, 1387–1396

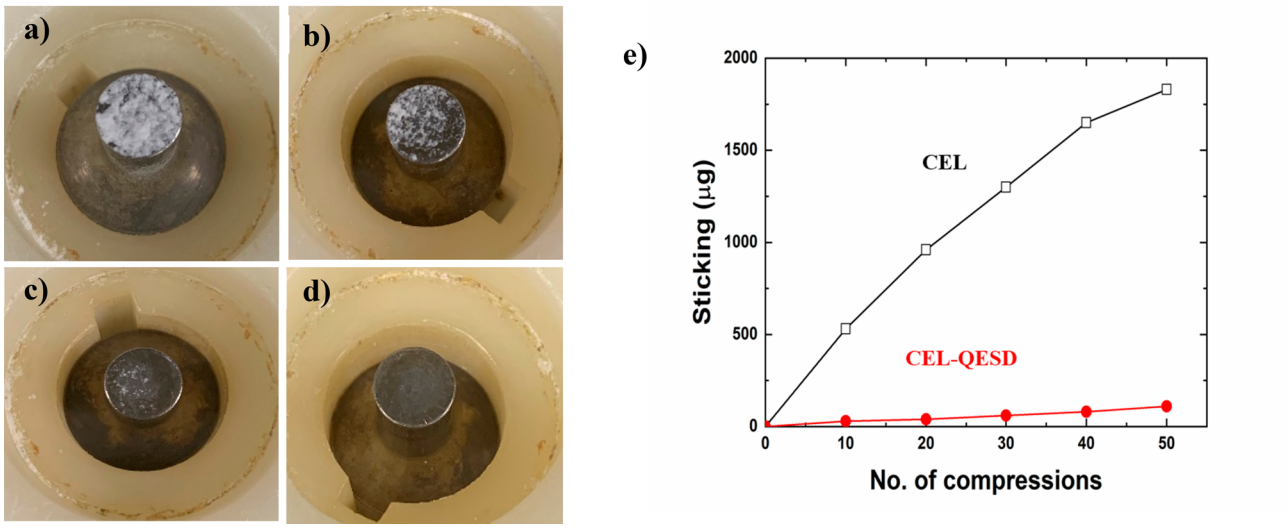

Figure 4. Punch-sticking propensity of CEL after compaction at 50 MPa: (a) as-received CEL, and CEL-QESD prepared from different concentrations of HPMC solutions (b) 0.1%, (c) 0.3%, and (d) 0.5%. (e) Quantitative sticking propensity assessment using formulated CEL powders (79.5% (w/w) Avicel PH102, 20% CEL, and 0.5% MgSt).

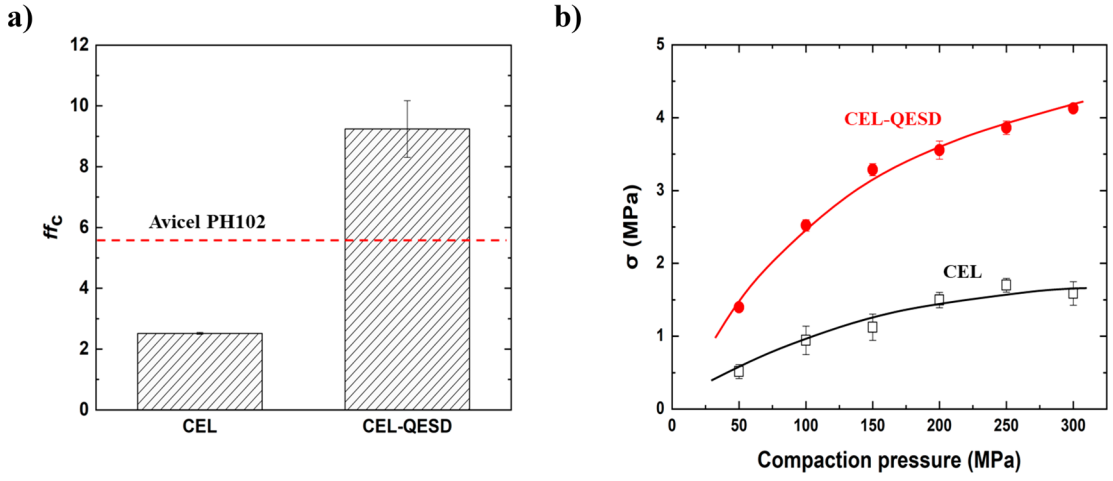

Figure 5. (a) Flowability (at 1 kPa preshear normal stress) and (b) tabletability of CEL-QESD (prepared from a 0.5% HPMC solution) as compared to as-received CEL.

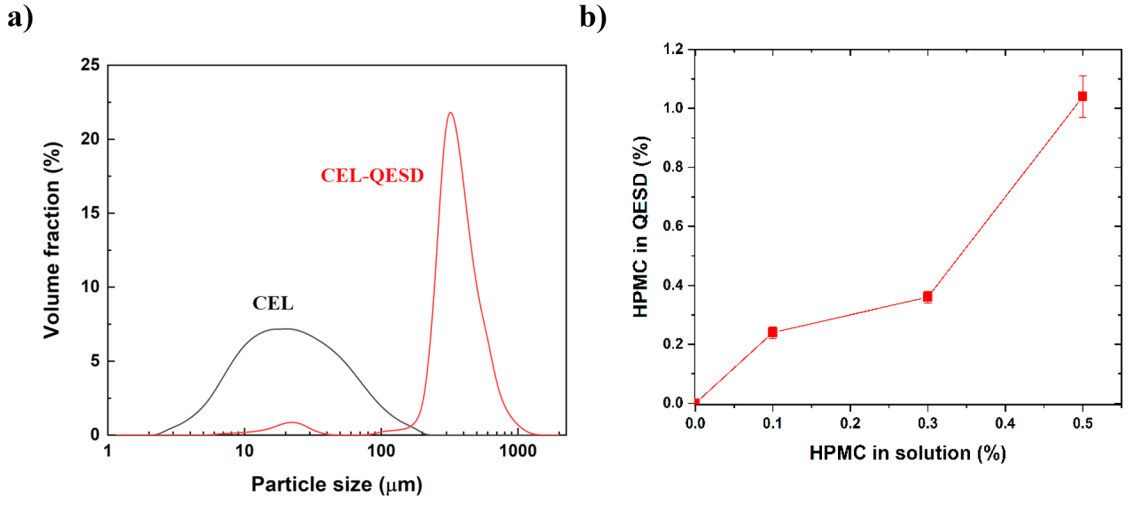

Figure 6. (a) Particle size distributions of as-received CEL and CEL-QESD powders and (b) HPMC content in solid CEL-QESD plotted as a function of the HPMC solution concentration (n = 3).

https://dx.doi.org/10.1021/acs.molpharmaceut.0c00086
Mol. Pharmaceutics 2020, 17, 1387−1396

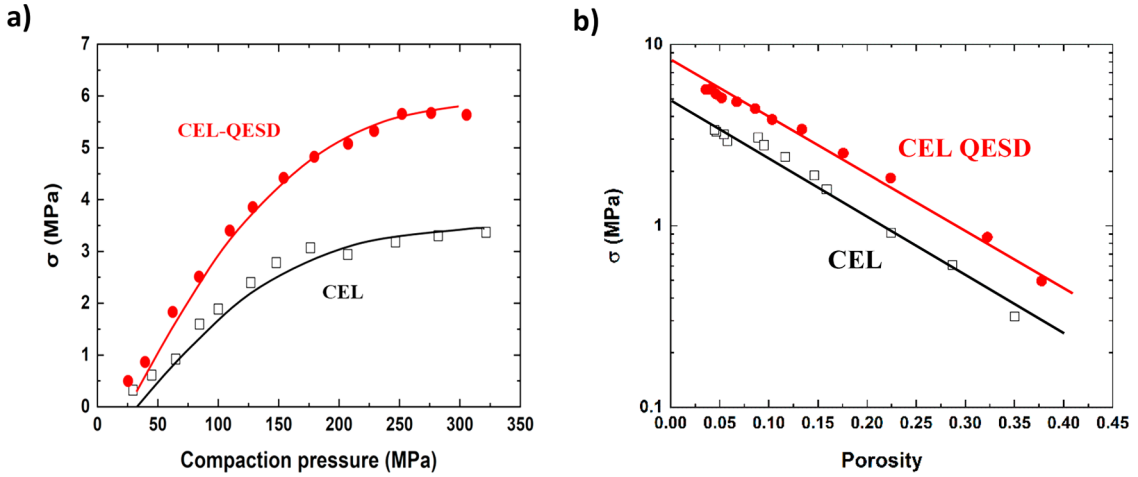

Figure 7. Compaction properties of as-received CEL and CEL-QESD (prepared from a 0.5% HPMC solution) formulations consisting of 79.5% of Avicel PH102, 20% of CEL, and 0.5% of MgSt: (a) tabletability and (b) compactibility.

solution exhibited a completely sticking free performance upon compression (Figure 4d).

Quantitative evaluation of punch-sticking propensity was carried out following an established method using formulated CEL,[4] comprising of Avicel PH102 (79.5 wt %), CEL (20 wt %), and MgSt (0.5 wt %). Results showed severe sticking propensity of the as-received CEL formulation, where >1.80 mg weight gain was recorded after 50 compressions (Figure 4e). In comparison, the CEL-QESD formulation only exhibited ∼0.10 mg weight gain after 50 compressions. Having established the successful reduction of punch sticking by spherical crystallization of CEL (CEL-QESD), we further examined the possible mechanisms in the following sections.

Solid Form and Residual Solvent. Both DSC (Figure S1a) and powder XRD (Figure S1b) analysis revealed that the CEL-QESD, derived from the 0.5% HMPC emulsion, and the as-received CEL exhibited the same thermal properties and crystal structure consistent with those of Form III. Thermogravimetric analyses further demonstrated the absence of detectable residual solvent in the CEL-QESD, since no sample weight loss was observed by increasing the temperature to 180 °C (Figure S1c). Therefore, the drastically reduced punch-sticking propensity cannot be ascribed to the presence of residual solvent or a change in CEL crystal form.

Manufacturability of CEL Powders. To evaluate the manufacturability of CEL-QESD, we characterized the flowability and tabletability. The flowability index ff_c of CEL-QESD was much higher than that of the as-received CEL (Figure 5a). By the measure of ff_c, CEL-QESD exhibited flowability suitable for high-speed tableting given that it flows better than Avicel PH102 while the as-received CEL did not (Figure 5a).[27] The improvement in powder flowability is an expected outcome for SA powders, due to the combination of the spherical morphology, smooth surface, and larger particle size of the CEL-QESD. Compared to the elongated fine crystals of the as-received CEL, CEL-QESD agglomerates were larger and more spherical. The spherical shape of the fine CEL-QESD particles in the range 10−40 μm (Figures 2 and 6a) suggests that they were likely resulted from the solidification of small droplets during the QESD process.

CEL-QESD also exhibited profoundly improved tabletability, with tablet tensile strengths more than 2-fold higher than those of as-received CEL (Figure 5b). Analysis of the results shows that the HMPC content in the CEL-QESD samples positively correlates with the HPMC concentration in the aqueous medium for QESD (Figure 6b). From the 0.5% HPMC solution, the CEL-QESD sample contained 1.04 ± 0.07% (w/w) HPMC (Figure 6b). Thus, the much improved tabletability may arise from a HMPC surface coating layer on the spherical agglomerate that facilitates the formation of a 3D bonding network upon powder compression, which has been shown to be extremely effective in improving powder tabletability.[28]

Consistent with the improved tabletability of the pure CEL-QESD powders (Figure 5b), the CEL-QESD formulation also exhibited much better tabletability than the CEL formulation (Figure 7a). According to the bonding area (BA)−bonding strength (BS) interplay model,[29] a higher tabletability is a consequence of large BA, higher BS, or both among the adjacent particles. BA and BS may be assessed using compressibility and compactibility plots, respectively. The nearly identical compressibility profiles of the two formulations (Figure S2) imply similar BA in tablets formed under the same compaction pressures. On the contrary, the compactibility profile of the CEL-QESD formulation was much higher than that of as-received CEL formulation, as shown by the higher σ at the same tablet porosity (Figure 7b), indicative of its higher apparent BS. Therefore, the higher tabletability of CEL-QESD formulation was driven by the higher BS. A higher BS among particles tends to correlate to a lower sticking propensity, because the interparticle adhesion is preferred to punch−particle adhesion, when the tablet is separated from the punch during tablet manufacturing.

Polymer Coating on CEL-QESD. To confirm the suspected surface HPMC coating, based on the improved tabletability, we first compared the surface properties of the different CEL and CEL-QESD particles. When viewed at a high magnification, the irregular and rough surfaces of CEL-QESD sharply contrasted the smooth surfaces of as-received CEL crystals (Figure 8). The presence of irregular surfaces can suggest the presence of noncrystalline (amorphous) material. However, given the high degree of CEL crystallinity observed by DSC and PXRD (Figure S1a,b), this possibility could be eliminated. Another possible origin of the irregular surface features of the CEL-QESD is the presence of a thin HPMC coating. Such a HPMC coating would be consistent with the

https://dx.doi.org/10.1021/acs.molpharmaceut.0c00086
Mol. Pharmaceutics 2020, 17, 1387−1396

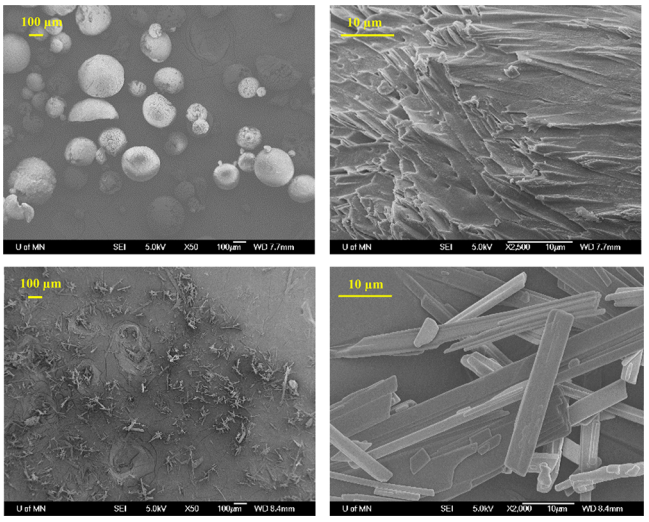

Figure 8. SEM images of CEL-QESD (top row) and as-received CEL (bottom row) at low (left column) and high (right column) magnifications. CEL-QESD was prepared from a 0.5% HPMC solution.

reduced punch-sticking propensity (Figure 4e), because it prevents the direct contact between CEL and punch.

The presence of a surface HPMC layer is further supported by the XPS data, which provides the surface elemental composition. The oxygen-rich nature of the cellulosic backbone of HMPC coupled with the unique occurrence of F and N in CEL (Figure 1) makes it possible to probe particle surface compositions by assessing the relative abundances of O, F, and N. Compared to the neat CEL powder, the CEL-QESD powder exhibited a significantly higher O 1s signal with concomitant suppression of the N 1s and F 1s signals (Figure 9a, Table 1). This result is consistent with the aforementioned notion that HMPC decorates the outer surface of the CEL-QESD. Upon compression into tablets, the CEL-QESD tablet also exhibited significantly lower F 1s and N 1s signals as compared to the tablets of the as-received CEL (Figure 9b, Table 1). This confirms the presence of a surface HPMC layer on the CEL-QESD particles and at the surface of tablet. Given the shallow takeoff angle (45°) employed in the XPS measurements, the observation of a F 1s signal in the CEL-QESD samples suggests that the minimum thickness of the HPMC layer coating the particle surfaces was thinner than the typical sampling depth of organic compounds by XPS, ~ 5 nm.[10,30] Otherwise, N and F in CEL would have not been detected if the HPMC layer was always thicker than the maximum sampling thickness by XPS.

Interactions between CEL and Polymers. To gain molecular-level insight into the very different performances of PVP, HPC, and HPMC in facilitating the QESD process of CEL (Figures 2 and 3), we sought to identify preferential intermolecular interactions between CEL and the various polymers using solution ^{1}H NMR (Figure 10). We directed our attention to changes in the appearance of the peaks associated with protons *ortho* to the aryl sulfonamide (H15 and 17), *meta* to the arylsulfonamide (H14 and H18), the sulfonamide $-NH_2$ (H23), tolyl protons (H7, H8, H10, H11, H12), and the pyrazole proton (H4) (see the numbering scheme in Figure 1). Although deuterium oxide is the most relevant solvent to investigate the drug-polymer interactions in the QESD process carried out in water, it could not be used because CEL is insoluble in it. Therefore, we employed DMSO-d_6 as the alternative solvent because of its high polarity and ability to dissolve both the polymers and CEL. The addition of HPMC (3 mg/mL) into a DMSO-d_6 solution of CEL (3 mg/mL) led to clear upfield shifts in the ^{1}H NMR resonances associated with H14 and H18 (δ 7.84−7.90 ppm), H15 and H17 (δ 7.52−7.60 ppm), H4, H7, H8, and H10 (δ 7.16−7.24 ppm), and H12 (δ 2.28−2.36 ppm). The observed upfield shifts of the ^{1}H NMR resonances suggest intermolecular hydrophobic interactions between CEL molecules and/or CEL and HMPC that result in increased electron densities at these positions.[31,32] We note that upfield shifts of the ^{1}H NMR resonances of aromatic compounds are often observed in their guest−host inclusion complexes with cyclodextrins;[33] the latter of which are cyclic saccharides that are structurally related to HPMC. The more hydrophilic HPC apparently resulted in much smaller shifts in the ^{1}H NMR resonances of CEL, indicating weaker intermolecular polymer/CEL interactions. Finally, very minimal peak shifts were observed with the most hydrophilic polymer PVP. These ^{1}H NMR observations lead us to conclude that hydrophobic interactions between the aryl and aliphatic moieties of the CEL and the permethylated HMPC additive drive their association in

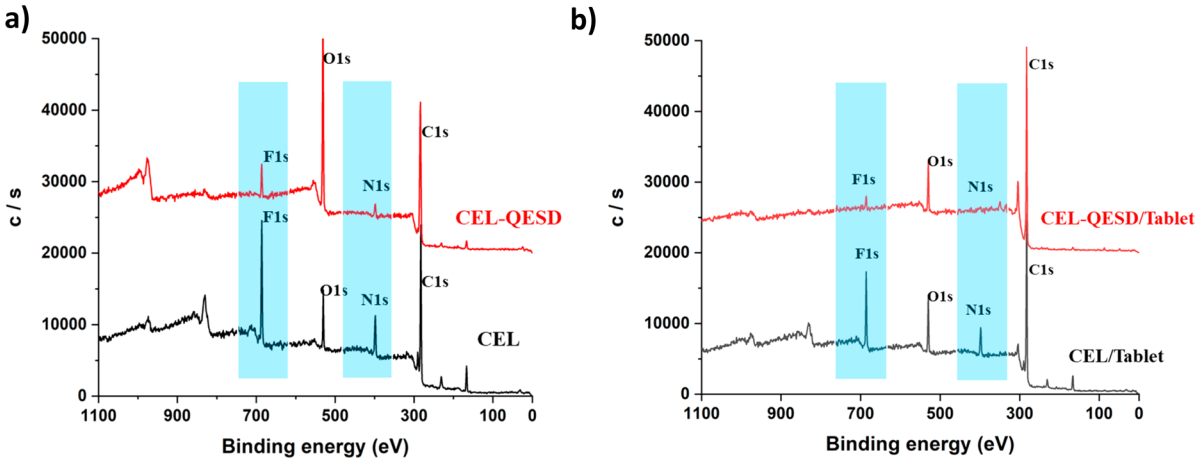

Figure 9. X-ray photoelectron spectral analysis of the particle surface elemental compositions of as-received CEL and CEL-QESD (prepared from a 0.5% HPMC solution), (a) powder, and (b) tablets.

https://dx.doi.org/10.1021/acs.molpharmaceut.0c00086
Mol. Pharmaceutics 2020, 17, 1387−1396

Table 1. Elemental Composition of Sample Surfaces

	CEL (%)	CEL-QESD (%)	CEL/tablet (%)	CEL-QESD/tablet (%)
O 1s	9.83 (±0.29)	32.00 (±2.65)	9.8 (±0.3)	11.20 (±1.51)
C 1s	69.13 (±1.5)	60.27 (±1.55)	69.1 (±1.5)	86.30 (±0.30)
N 1s	8.93 (±0.32)	3.37 (±0.42)	3.4 (±0.4)	0
F 1s	9.57 (±0.95)	3.17 (±0.70)	9.1 (±1.3)	2.07 (±1.44)

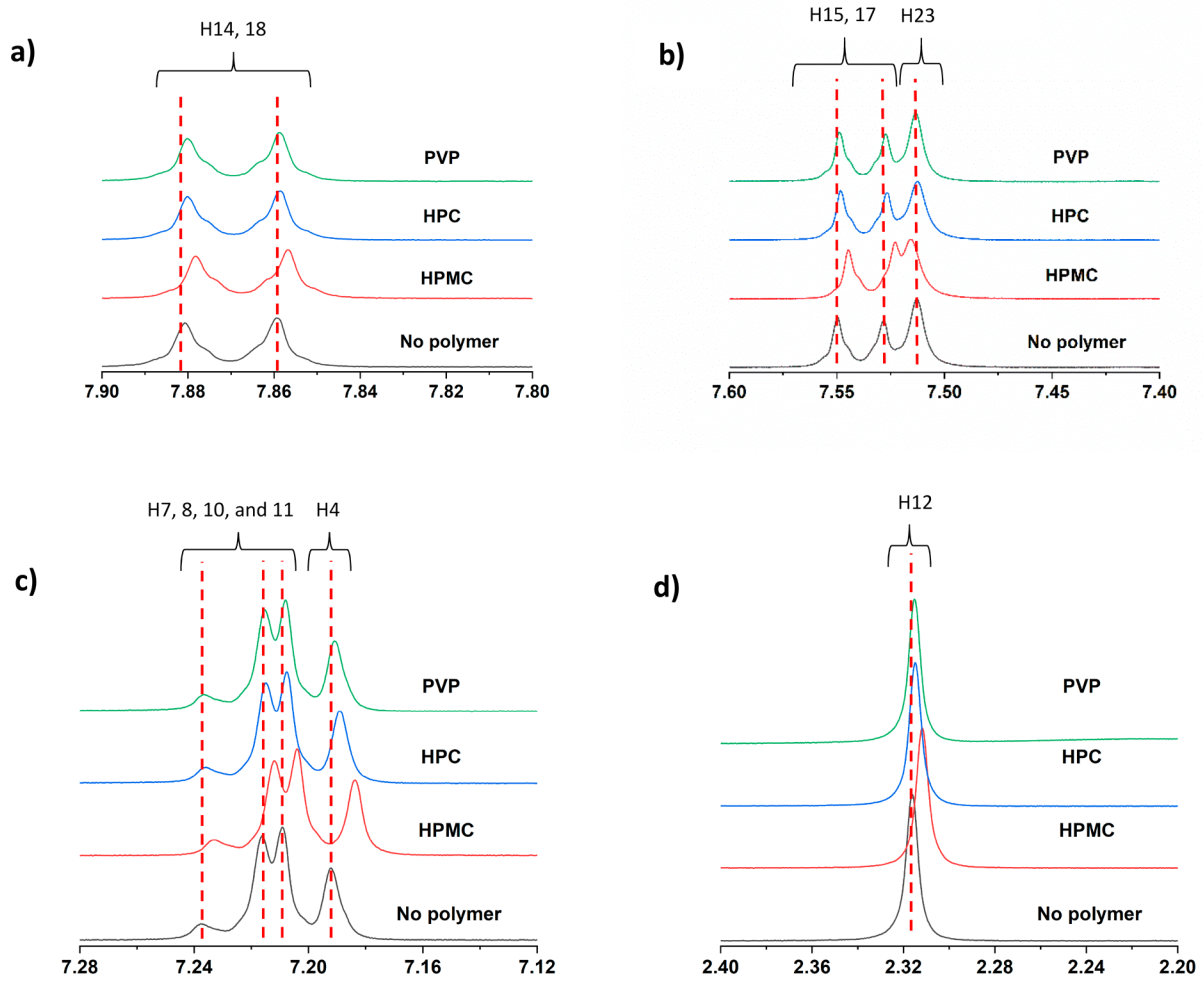

Figure 10. 1D ^{1}H NMR spectra of CEL (3 mg/mL) with different polymer additives (3 mg/mL) in DMSO-d_6 over the chemical shift ranges (a) δ 7.80−7.90 ppm, (b) δ 7.40−7.60 ppm, (c) δ 7.12−7.28 ppm, and (d) δ 2.20−2.40 ppm. The numbering of the resonances corresponds to that given in Figure 1.

DMSO-d_6 solutions. We note that HMPC addition drove a downfield shift of the peak associated with H23 (δ 7.50−7.52 ppm). This last downfield shift of peaks indicated a decrease in electron density at these protons, suggestive of sulfonamide hydrogen bond donation to either the HPMC or to other CEL molecules that are hydrophobically associated with the polymer. No such peak shifts were observed with the more hydrophilic HPC and PVP additives, even though PVP is solely a hydrogen bond acceptor that could form complementary interactions with free CEL. This last observation suggests that intermolecular interactions between hydrophobically associated CEL molecules along a HPMC chain drive substantial changes in the chemical environment around the amino group that lead to the observed chemical shift.

The NMR data shown in Figure 10 suggests that CEL−polymer association strength follows the descending order of HPMC ≫ HPC > PVP. This order is consistent with their CEL emulsion stabilization abilities discerned from the time-dependent optical micrographs (Figure 3). Thus, hydrophobic association between the CEL and HPMC appears to play a critical role in stabilizing the quasi-emulsion and enabling the formation of spherical agglomerates. Compared to that observed by ^{1}H NMR in DMSO-d_6, the hydrophobic association is likely stronger in the higher polarity H_2O during the QESD process. HPMC chains may thus be driven from the aqueous medium to adsorb onto the emulsion droplet interfaces, leading to their temporary stabilization that allows for spherical agglomerate formation with a thin HPMC coating. These findings concur with previous studies that demonstrated the ability of HPMC to form specific intermolecular interactions with CEL to significantly reduce

https://dx.doi.org/10.1021/acs.molpharmaceut.0c00086
Mol. Pharmaceutics 2020, 17, 1387−1396

the crystal growth in a supersaturated solution,[34] whereas the more hydrophilic PVP did not.[35]

CONCLUSIONS

We have shown that the strength of the intermolecular interactions between CEL and HPMC, HPC, and PVP is positively correlated with their ability to facilitate spherical agglomeration of CEL by the QESD process. The HPMC enabled CEL-QESD agglomerates exhibit significantly reduced punch-sticking propensity of CEL with substantially improved tabletability and flowability. These significant enhancements in CEL powder properties are attributed to QESD emulsion droplet stabilization by HPMC adsorption to the droplet surfaces. This results in a thin HPMC coating on the surfaces of the resulting CEL-QESD particles, which reduces punch-sticking propensity by forming a physical barrier to separate CEL from the punch surface during compression. This first successful example of reducing punch-sticking propensity of a highly sticky API by QESD, coupled with molecular-level insight into the underlying mechanism, adds another powerful particle engineering strategy to the arsenal of tools that can be used to solve common tablet manufacturing problems.

ASSOCIATED CONTENT

Supporting Information

The Supporting Information is available free of charge at https://pubs.acs.org/doi/10.1021/acs.molpharmaceut.0c00086.

Figures of DSC, TGA, PXRD patterns, and compressibility plots (PDF)

AUTHOR INFORMATION

Corresponding Author

Changquan Calvin Sun − *Pharmaceutical Materials Science and Engineering Laboratory, Department of Pharmaceutics, College of Pharmacy, University of Minnesota, Minneapolis, Minnesota 55455, United States;* orcid.org/0000-0001-7284-5334; Phone: 612-624-3722; Email: sunx0053@umn.edu; Fax: 612-626-2125

Authors

Hongbo Chen − *Pharmaceutical Materials Science and Engineering Laboratory, Department of Pharmaceutics, College of Pharmacy, University of Minnesota, Minneapolis, Minnesota 55455, United States*

Shubhajit Paul − *Pharmaceutical Materials Science and Engineering Laboratory, Department of Pharmaceutics, College of Pharmacy, University of Minnesota, Minneapolis, Minnesota 55455, United States*

Hongyun Xu − *Department of Chemical Engineering and Materials Science, University of Minnesota, Minneapolis, Minnesota 55455, United States;* orcid.org/0000-0002-2406-9024

Kunlin Wang − *Pharmaceutical Materials Science and Engineering Laboratory, Department of Pharmaceutics, College of Pharmacy, University of Minnesota, Minneapolis, Minnesota 55455, United States;* orcid.org/0000-0003-1382-4933

Mahesh K. Mahanthappa − *Department of Chemical Engineering and Materials Science, University of Minnesota, Minneapolis, Minnesota 55455, United States;* orcid.org/0000-0002-9871-804X

Complete contact information is available at: https://pubs.acs.org/10.1021/acs.molpharmaceut.0c00086

Notes

The authors declare no competing financial interest.

ACKNOWLEDGMENTS

H.C. thanks the Chinese Scholarship Council for partial financial support. H.C. also acknowledges partial support by a David Grant and Marilyn Grant Fellowship in Physical Pharmacy (2019−2020), Department of Pharmaceutics, University of Minnesota. H.X. and M.K.M. gratefully acknowledge the National Science Foundation DMR-1708874. XPS analyses were performed in the College of Science and Engineering Characterization Facility at the University of Minnesota, which also receives partial support from the National Science Foundation through the UMN MRSEC (DMR-1420013).

REFERENCES

(1) Chen, H.; Aburub, A.; Sun, C. C. Direct compression tablet containing 99% active ingredient—a tale of spherical crystallization. *J. Pharm. Sci.* **2019**, *108*, 1396−1400.

(2) Lakshman, J. P.; Kowalski, J.; Vasanthavada, M.; Tong, W. Q.; Joshi, Y. M.; Serajuddin, A. T. Application of melt granulation technology to enhance tabletting properties of poorly compactible high-dose drugs. *J. Pharm. Sci.* **2011**, *100*, 1553−1565.

(3) Cai, L.; Farber, L.; Zhang, D.; Li, F.; Farabaugh, J. A new methodology for high drug loading wet granulation formulation development. *Int. J. Pharm.* **2013**, *441*, 790−800.

(4) Paul, S.; Taylor, L. J.; Murphy, B.; Krzyzaniak, J.; Dawson, N.; Mullarney, M. P.; Meenan, P.; Sun, C. C. Mechanism and kinetics of punch sticking of pharmaceuticals. *J. Pharm. Sci.* **2017**, *106*, 151−158.

(5) Wang, J. J.; Guillot, M. A.; Bateman, S. D.; Morris, K. R. Modeling of adhesion in tablet compression. II. Compaction studies using a compaction simulator and an instrumented tablet press. *J. Pharm. Sci.* **2004**, *93*, 407−417.

(6) Chattoraj, S.; Daugherity, P.; McDermott, T.; Olsofsky, A.; Roth, W. J.; Tobyn, M. Sticking and picking in pharmaceutical tablet compression: An IQ consortium review. *J. Pharm. Sci.* **2018**, *107*, 2267−2282.

(7) Paul, S.; Taylor, L. J.; Murphy, B.; Krzyzaniak, J. F.; Dawson, N.; Mullarney, M. P.; Meenan, P.; Sun, C. C. Powder properties and compaction parameters that influence punch sticking propensity of pharmaceuticals. *Int. J. Pharm.* **2017**, *521*, 374−383.

(8) Abdel-Hamid, S.; Betz, G. A novel tool for the prediction of tablet sticking during high speed compaction. *Pharm. Dev. Technol.* **2012**, *17*, 747−754.

(9) Roberts, M.; Ford, J. L.; MacLeod, G. S.; Fell, J. T.; Smith, G. W.; Rowe, P. H. Effects of surface roughness and chrome plating of punch tips on the sticking tendencies of model ibuprofen formulations. *J. Pharm. Pharmacol.* **2003**, *55*, 1223−1228.

(10) Paul, S.; Wang, C.; Wang, K.; Sun, C. C. Reduced punch sticking propensity of acesulfame by salt formation: Role of crystal mechanical property and surface chemistry. *Mol. Pharmaceutics* **2019**, *16*, 2700−2707.

(11) Paul, S.; Sun, C. C. Modulating sticking propensity of pharmaceuticals through excipient selection in a direct compression tablet formulation. *Pharm. Res.* **2018**, *35*, 113.

(12) Al-Karawi, C.; Leopold, C. S. A comparative study on the sticking tendency of ibuprofen and ibuprofen sodium dihydrate to differently coated tablet punches. *Eur. J. Pharm. Biopharm.* **2018**, *128*, 107−118.

(13) Simmons, D. M.; Gierer, D. S. A material sparing test to predict punch sticking during formulation development. *Drug Dev. Ind. Pharm.* **2012**, *38*, 1054−1060.

(14) Kawashima, Y.; Niwa, T. Preparation of controlled-release microspheres of ibuprofen with acrylic polymers by a novel quasi-emulsion solvent diffusion method. *J. Pharm. Sci.* **1989**, *78*, 68−72.
(15) Sano, A.; Kuriki, T.; Kawashima, Y.; Takeuchi, H.; Hino, T.; Niwa, T. Particle design of tolbutamide by the spherical crystallization technique. III. Micromeritic properties and dissolution rate of tolbutamide spherical agglomerates prepared by the quasi-emulsion solvent diffusion method. *Chem. Pharm. Bull.* **1990**, *38*, 733−739.
(16) Kawashima, Y.; Niwa, T.; Takeuchi, H.; Hino, T.; Itoh, Y.; Furuyama, S. Characterization of polymorphs of tranilast anhydrate and tranilast monohydrate when crystallized by two solvent change spherical crystallization techniques. *J. Pharm. Sci.* **1991**, *80*, 472−478.
(17) Morishima, K.; Kawashima, Y.; Kawashima, Y.; Takeuchi, H.; Niwa, T.; Hino, T. Micromeritic characteristics and agglomeration mechanisms in the spherical crystallization of bucillamine by the spherical agglomeration and the emulsion solvent diffusion methods. *Powder Technol.* **1993**, *76*, 57−64.
(18) Tahara, K.; O'Mahony, M.; Myerson, A. S. Continuous spherical crystallization of albuterol sulfate with solvent recycle system. *Cryst. Growth Des.* **2015**, *15*, 5149−5156.
(19) Tahara, K.; Kono, Y.; Myerson, A. S.; Takeuchi, H. Development of continuous spherical crystallization to prepare fenofibrate agglomerates with impurity complexation using mixed-suspension, mixed-product removal crystallizer. *Cryst. Growth Des.* **2018**, *18*, 6448−6454.
(20) Ray, W. A.; Stein, C. M.; Daugherty, J. R.; Hall, K.; Arbogast, P. G.; Griffin, M. R. COX-2 selective non-steroidal anti-inflammatory drugs and risk of serious coronary heart disease. *Lancet* **2002**, *360*, 1071−1073.
(21) Wang, K.; Mishra, M. K.; Sun, C. C. Exceptionally elastic single-component pharmaceutical crystals. *Chem. Mater.* **2019**, *31*, 1794−1799.
(22) Paul, S.; Chang, S.-Y.; Sun, C. C. The phenomenon of tablet flashing — its impact on tableting data analysis and a method to eliminate it. *Powder Technol.* **2017**, *305*, 117−124.
(23) Fell, J. T.; Newton, J. M. Determination of tablet strength by the diametral-compression test. *J. Pharm. Sci.* **1970**, *59*, 688−691.
(24) Ryshkewitch, E. Compression strength of porous sintered alumina and zirconia. *J. Am. Ceram. Soc.* **1953**, *36*, 65−68.
(25) Chen, M.-H.; Bergman, C. J. Method for determining the amylose content, molecular weights, and weight- and molar-based distributions of degree of polymerization of amylose and fine-structure of amylopectin. *Carbohydr. Polym.* **2007**, *69*, 562−578.
(26) Gapper, L. W.; Copestake, D. E. J.; Otter, D. E.; Indyk, H. E. J. A.; Chemistry, B. Analysis of bovine immunoglobulin G in milk, colostrum and dietary supplements: A review. *Anal. Bioanal. Chem.* **2007**, *389*, 93−109.
(27) Sun, C. C. Setting the bar for powder flow properties in successful high speed tableting. *Powder Technol.* **2010**, *201*, 106−108.
(28) Shi, L.; Sun, C. C. Transforming powder mechanical properties by core/shell structure: Compressible sand. *J. Pharm. Sci.* **2010**, *99*, 4458−4462.
(29) Osei-Yeboah, F.; Chang, S.-Y.; Sun, C. C. J. P. R. A critical examination of the phenomenon of bonding area - bonding strength interplay in powder tableting. *Pharm. Res.* **2016**, *33*, 1126−1132.
(30) Tanuma, S.; Powell, C. J.; Penn, D. R. Calculations of electron inelastic mean free paths. II. Data for 27 elements over the 50−2000 ev range. *Surf. Interface Anal.* **1991**, *17*, 911−926.
(31) Chen, Y.; Pui, Y.; Chen, H.; Wang, S.; Serno, P.; Tonnis, W.; Chen, L.; Qian, F. Polymer-mediated drug supersaturation controlled by drug-polymer interactions persisting in an aqueous environment. *Mol. Pharmaceutics* **2019**, *16*, 205−213.
(32) Jasani, M. S.; Kale, D. P.; Singh, I. P.; Bansal, A. K. Influence of drug-polymer interactions on dissolution of thermodynamically highly unstable cocrystal. *Mol. Pharmaceutics* **2019**, *16*, 151−164.
(33) Schneider, H.-J.; Hacket, F.; Rüdiger, V.; Ikeda, H. Nmr studies of cyclodextrins and cyclodextrin complexes. *Chem. Rev.* **1998**, *98*, 1755−1786.
(34) Ilevbare, G. A.; Liu, H.; Edgar, K. J.; Taylor, L. S. Impact of polymers on crystal growth rate of structurally diverse compounds from aqueous solution. *Mol. Pharmaceutics* **2013**, *10*, 2381−2393.
(35) Xie, T.; Taylor, L. S. Dissolution performance of high drug loading celecoxib amorphous solid dispersions formulated with polymer combinations. *Pharm. Res.* **2016**, *33*, 739−750.

https://dx.doi.org/10.1021/acs.molpharmaceut.0c00086
Mol. Pharmaceutics 2020, 17, 1387−1396